Employing a novel bioelastomer to toughen polylactide

Hailan Kang,[†] Bo Qiao,[†] Runguo Wang,[†] Zhao Wang,[†] Liqun Zhang,[,†,‡] Jun Ma,[*,§] Phil Coates[£]*

[†]State Key Laboratory of Organic-Inorganic Composites; [‡]Key Laboratory of Beijing City for Preparation and Processing of Novel Polymer Materials, Beijing University of Chemical Technology, 100029, P. R. China

[§]School of Advanced Manufacturing and Mechanical Engineering, University of South Australia, SA5095, Australia

[£]School of Engineering, Design &Technology, Bradford University, BD7 1DP, UK

CORRESPONDING AUTHOR FOOTNOTE: Correspondences should be addressed to Prof L. Q. Zhang or Dr J. Ma at ZhangLQ@mail.buct.edu.cn or Jun.Ma@unisa.edu.au.

ABSTRACT. Biodegradable, biocompatible polylactide (PLA) synthesized from renewable resources has attracted extensive interests over the past decades and holds great potential to replace many petroleum-derived plastics. With no loss of biodegradability and biocompatibility, we highly toughened PLA using a novel bioelastomer (BE)–synthesized from biomass diols and diacids. Although PLA and BE are immiscible, BE particles of ~1 μm in diameter are uniformly dispersed in the matrix, and this indicates some compatibility between PLA and BE. BE significantly increased the cold crystallization ability of PLA, which was valuable for practical processing and performance. SEM micrographs of fracture surface showed a brittle-to-ductile transition owing to addition of BE. At 11.5 vol%, notched Izod impact strength improved from 2.4 to 10.3 kJ/m^2, 330% increment; the increase is superior to previous toughening effect by using petroleum-based tougheners.

KEYWORDS. Polylactide, Bioelastomer, Toughness

Introduction

Biobased polymers from renewable resources have received considerable interests from academia and industry in recent years, due to environmental concerns for ever-declining petroleum resources [1-3]. The use of biobased polymers is currently a major alternative to conventional petroleum-based polymers, and will provide a solution to the environment problem of plastic wastes [4]. Polylactide (PLA) is a polymer produced from renewable resources such as corn on a commercial scale [5]; it is a thermoplastic aliphatic polyester and has been proven viable in replacing petroleum-based plastics in some applications [6]. However, PLA is inherently brittle, which severely limits its application in industries. Toughening PLA has thus attracted great interests.

Low-molecular weight plasticizers toughened PLA moderately but this was obtained at the cost of losing stiffness [7-11]. Inorganic fillers such as clay improved toughness little, although enhancing stiffness obviously [12-14]. The most practical and economic used methods for toughening PLA is to adopt flexible polymers or elastomers. Poly (ε-caprolactone) (PCL) was the earliest polymer used for toughening PLA [15-21]. Since PCL and PLA are not compatible, compatibilizers such as PLLA-PCL-PLLA triblock copolymer have been developed [18]; it produced an improvement in notched Charpy impact strength from 1.1 to 3.7 kJ/m^2 at 30 wt% PCL. Compatible PLA/PCL blends were prepared through reactive processing induced by catalysts [19] or crosslinkers [20,21]. Jiang et al. [22] improved Izod impact strength by 170 % via mixing PLA with 20 wt% poly (butylene adipate-co-terephthalate) (PBAT). Li et al. [23] prepared PLA/poly(ether) urethane (PU) blends with improved impact strength from 64 kJ/m^2 to 315 kJ/m^2. Zhang et al. [24] used polyamide elastomer (PAE) to toughen PLA, resulting in a increase in elongation at break from 5.1% to 194.6% at 10 wt% PAE. PLA was blended with four synthetic rubbers, including ethylene–propylene copolymer (EPM), ethylene–acrylic rubber (AEM), acrylonitrile–butadiene rubber (NBR), and isoprene rubber (IR), but toughening was only achieved by PLA/NBR blend with a 1.8 times higher value of Izod impact strength in comparison with PLA [25]. Even though these polymers toughened PLA effectively, unfortunately these polymers are either nonrenewable or nondegradable. A recent trend for toughening PLA is to

adopt degradable, renewable polymers, including starch [26,27], poly (butylene succinate) (PBS) [28,29], poly (hydroxyalkanoates) [30,31], polymerized soybean oil [32] and polyamide11 (PA11) [33]; these are fabricated from renewable resources, and upon disposal are able to degrade completely in the environment within dozens of years. Shibata et al. [29] toughened PLLA by poly (butylene succinate-co-$_L$-lactate) (PBSL) and poly (butylene succinate) (PBS); at 10 wt%, these two tougheners achieved 160% and 120% higher elongation at break, respectively. Robertson et al. [32] achieved 400% and 600% increase in elongation at break and tensile toughness by using polymerized soybean oil, respectively. However, most tougheners derived from renewable resources are less effective than those derived from petroleum resources in improving the PLA toughness. On the other hand, most studies used the improved elongation at break rather than the notched impact strength to gauge the toughening effects, while the impact testing is far more useful in practice. Therefore, the challenge is to develop biocompatible, highly toughened PLA blends which retain both completely renewable origins and ultimate degradability if necessary [34].

Considering the fact that elastomers have commonly been adopted as a second-phase polymer for toughening many kinds of brittle polymer materials, such as epoxy [35,36], polypropylene [37], poly(methyl methacrylate) [38], and so on, it becomes very interesting and important to look for or design/synthesize the new biobased and biocompatible elastomers to toughen PLA. Recently we have developed novel bioelastomers from polymerizing commercial biobased monomers—sebacic acid, itaconic acid, succinic acid, propanediol and butanediol—all of which are derived from renewable resources [39]. While possessing complete biocompatibility, these elastomers exhibit satisfactory elasticity and good mechanical strength. It is noteworthy that the repeat units of these bioelastomers are based on ester groups, implying some compatibility with other ester bond-based polymers such as PLA [7,28]. Thus, a hypothesis made in this study is that our bioelastomers have great potential for toughening PLA.

In this work, we will significantly toughen PLA by compounding with our synthetic bioelastomer. The morphology, thermal behaviors, rheological properties and mechanical properties of the blends will be extensively investigated.

Experimental Section

Raw materials. Itaconic acid (IA) (purity 99.0%), succinic acid (SA) (purity 99.0%), 1, 3-propanediol (PDO) (purity 99.0%) and 1, 4-butanediol (BDO) (purity 99.0%) were purchased from Alfa Aesar. Sebacic acid (SeA) (purity 99.0%) was obtained from Guangfu Fine Chemical Institute of Tianjin. Tetrabutyl orthotitanate (TBOT), hydroquinone and phosphorous acid were supplied by Fluka, Beijing Yili Fine Chenical Co. Ltd, and Sinopharm Chemical Reagent Co. Ltd, respectively. Polylactide (PLA, 5051x) was provided by Natureworks USA. It exhibits a weight-average molecular weight of ~159,000 g/mol, a polydispersity index of 1.67 (GPC analysis), and a glass transition temperature and melting point of 60 ^{o}C and 152 ^{o}C (DSC analysis), respectively. The liquid silicone rubber (SiR) was commercial products and the number-average molecular weight is 20,000 g/mol. The PLA and BE chemical structures are shown in Fig. 1.

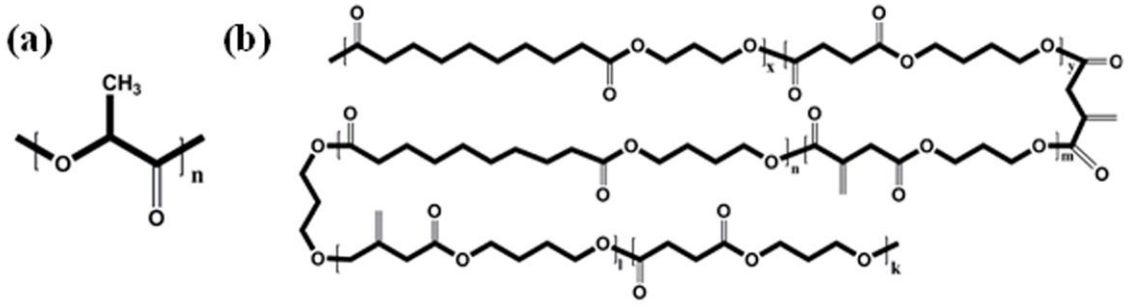

Fig. 1. Chemical structures of (a): Polylactide (PLA) and (b): Bioelastomer (BE).

Synthesis of BE. Our bioelastomer (BE) was synthesized according to our recent work [39]. In brief, we charged PDO (12.54 g, 0.165 mol), BDO (14.85 g, 0.165 mol), SA (15.04g, 0.1275 mol), IA (5.85 g, 0.045 mol), SeA (25.76 g, 0.1275 mol), and inhibitors hydroquinone (0.0296 g) and phosphorous acid (0.0074 g) into a 100-ml three-neck flask. The mixture was purged with nitrogen and then heated at 180 ^{o}C for 2 h; the water formed during the reaction was distilled off. In the second phase, after adding TBOT (0.05 wt% relative to the quantity of all reactants) as the catalyst, the mixture was heated to 220 ^{o}C under reduced pressure (<300 Pa) for 3–4 h until the Weisenberg effect was found. The resulting

product BE exhibits a weight-average molecular weight of ~181,000 g/mol, a polydispersity index of 3.7 (GPC analysis) and a glass transition temperature of -56 ºC (DSC analysis).

Sample Preparation. PLA and BE were dried in a vacuum oven at 60 ºC for 24 h prior to use. Blends were prepared by melt-mixing BE at different weight ratios (0, 5, 10, 15, and 20 wt%) with PLA for 10 min using a Haake Remix (Remix 600p, Thermal Electron Co., USA) at 170 ºC with a rotary speed of 80 rpm. All the samples were finally hot-pressed under 10 MPa at 190 ºC for 5 min to produce 1-mm thick sheets. The density of PLA and BE were 1.24 g/cm^3 and 1.06 g/cm^3; thus, we were able to convert wt% to vol%.

Characterization

The average molecular weight and polydispersity index were determined by gel permeation chromatographic (GPC) measurements on a Waters Breeze instrument equipped with three water columns (Steerage HT3 HT5 HT6E) using tetrahydrofuran as the eluent (1 ml/min) and a Waters 2410 refractive index detector. Polystyrene standard was used for calibration.

Dynamic mechanical thermal analysis was carried out with a V Dynamic Mechanical Thermal Analyzer (Rheometric Scientific Co.) with a tension mode at 1 Hz and 3 ºC/min from -100–150 ºC. Differential scanning calorimetry measurements were performed with a Mettler-Toledo DSC instrument under nitrogen. All samples were heated to 200 ºC at 50 ºC /min and kept isothermal for 5 min to remove previous thermal history. Then they were cooled to -100 ºC at 10 ºC /min, and reheated up to 200 ºC at 10 ºC /min to determine glass transition temperature (T_g), cold crystallization temperature (T_{cc}) and melting temperature (T_m). Isothermal crystallization behaviors of PLA/BE blends were also evaluated using DSC by premelting samples at 200 ºC for 5 min, followed by rapid cooling to -100 ºC and heating to 125 ºC at 50 ºC /min. Then the samples were kept at 125 ºC for 30 min to allow cold crystallization from the quiescent melt. The exothermic curves of heat flow as a function of time were recorded. X-ray diffraction (XRD) measurements were carried out on a D/Max2500 VB2+/PC X-ray diffractometer (Rigaku, Japa) with a Cu target radiation for a 2θ range of 5–50º at an angular resolution of 0.05º. The XRD samples were treated with the following procedures: (i) all samples were heated to

200 ºC and kept for 5 min; (ii) then they were cooled to room temperature at 10 ºC /min. The heating/cooling process was *in situ* conducted during the testing.

The morphology of the blends was determined by scanning electron microscopy (S4700, Hitachi Co., Japan) at 5 kV. After immersing in liquid nitrogen for 10 min, notched samples were fractured by a vice, and then surface-coated with a thin gold layer. The number-average particle diameter (D_n) was determined by Nano Measurer 1.2 and 100 particles were analyzed per sample. The etched samples were immersed into toluene for 10 min at room temperature, and then dried under 50 ºC in the vacuum oven. Transmission electron microscopy was performed on an H-800-1 transmission electron microscope (Hitachi Co., Japan) at 200 kV. The samples were ultramicrotomed at -100 ºC to produce sections of 60 nm in thickness, and then stained by RuO_4 at room temperature for 20 min.

Rheological properties were measured by Advanced Rheometrics Expansion System (ARES-G2) with a 25 mm plate-plate arrangement. The test was conducted in the frequency 0.01 to 100 rad/s at strain rate 5% and at 170 ºC.

Type-V dumbbell-shaped specimens were molded and measured at room temperature according to ASTM D638, by using a CMT 4104 Electrical Tensile Instrument (Shenzhen SANS Test Machine Co., Ltd. China) at 5 mm/min. The notched Izod impact strength was performed using Ceast, Resil Impactor machine according to GB/T 1843-2008. A-shaped notches with a radius of around 0.2 mm in the impact bars were produced by a Ceast notcher. At least five specimens were tested for an average value.

Results and Discussion

3.1 Morphology

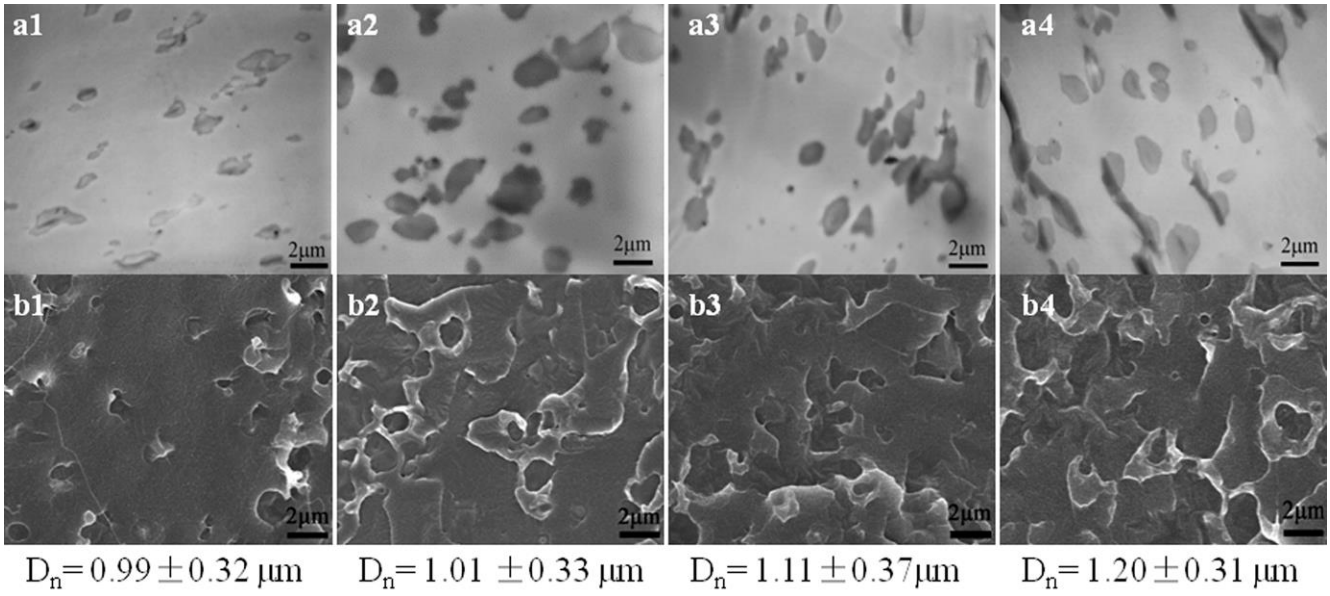

Fig. 2. Micrographs of PLA/BE blends with (a1, b1) 5.8 vol% BE, (a2, b2) 11.5 vol% BE, (a3, b3) 17.1 vol% BE, and (a4, b4) 22.6 vol% BE. a: TEM micrographs; b: SEM micrographs; D_n: The number-average particle diameter.

The phase morphology studies can provide the relationship of the microstructure and mechanical properties. Therefore, the detailed phase morphology was evaluated of polylactide (PLA)/bioelastomer (BE) blends using Transmission electron microscopy (TEM) and Scanning electron microscopy (SEM) In Fig. 2a1–4, BE was observed as the dark phase in TEM micrographs, because flexible BE macromolecules have more double bonds than PLA matrix and these double bonds readily react with RuO_4 [40,41]. While phase separation is evident at all fractions, BE particles are uniformly dispersed in PLA matrix. Statistics from 100 randomly selected particles at each fraction show that the number-average particle diameter (D_n) increases from 0.99 μm at 5.8 vol% to 1.20 μm at 22.6 vol%. In Fig. 2b1–4, a number of voids observed might be caused by the removal of dispersion phase of BE when these specimens were frozen-fractured. These TEM and SEM micrographs demonstrate the following features of PLA/BE blends: (i) these BE particles have an average diameter of ~1 μm, and seem to

disperse uniformly in matrix; and (ii) the particle geometry is irregular and it is difficult to observe these particles under SEM.

To identify what caused the irregularity of BE particles, an identical fabrication process was employed to prepare PLA/silicone rubber (SiR) blend as a comparison. In Fig. S1, large spherical SiR particles of 7.7 μm in diameter (D_n) are clearly seen, completely different to those BE particles in PLA. Many factors determine the dispersion particle size in blend, such as compatibility, viscosity match and shear rate; of these, compatibility is the most dominant factor. If two components in a binary blend have good compatibility, the dispersion particles would uniformly disperse in the matrix with relatively narrow particle size distribution, and vice versa [42-45]. The far lower particle size of BE may indicate an improved compatibility between BE and PLA, and this will be further discussed in the following analysis. If a dispersion polymer is incompatible with PLA, then the polymer would exist as spherical particles to reduce surface tension; the irregular geometry of BE particles shows that our PLA/BE blend is different to PLA/SiR blend, implying that PLA and BE have good interfacial interaction.

3.2 Dynamic Mechanical Thermal Analysis

Dynamic mechanical thermal analysis (DMTA) was adopted to investigate the miscibility and phase interaction of the PLA/BE system. Glass transition temperature (T_g) is a temperature at which there is an obvious enhancement in motion of large segments of molecular chains with increasing temperature. T_g is commonly used to gauge polymer-polymer miscibility in a blend by comparing the blend T_g with the T_gs of neat polymers [22-24]. In Fig. 3a wherein tan δ curves display as a function of temperature, the temperature at the peak of each tan δ curve represents glass transition temperature (T_g). All blends demonstrate two T_gs, indicating that the blends are immiscible. However, these T_gs shifted 3–9ºC inwards towards each other, implying an improved compatibility between PLA and BE through melt-compounding. This is probably caused by a certain degree of macromolecular affinity between PLA and BE, because of the similar chemical natures of the PLA and BE.

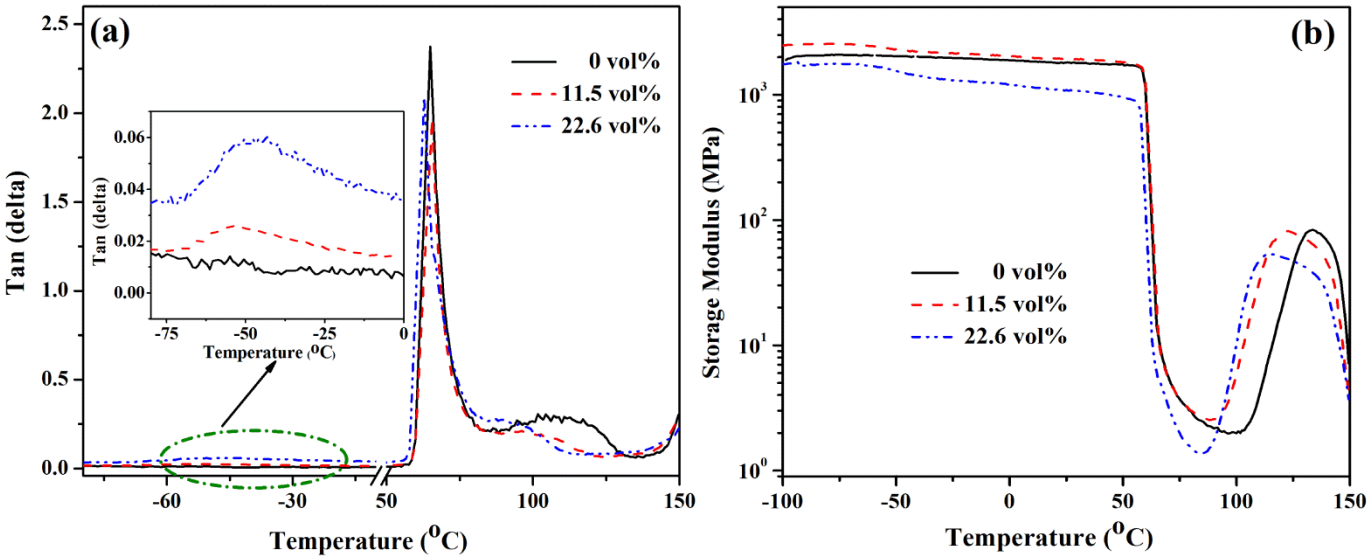

Fig. 3. Dynamic viscoelastic curves of PLA/BE blends with different amounts of BE: (a) tan δ versus temperature; (b) storage modulus versus temperature.

In Fig. 3b, the tensile storage modulus (E') of neat PLA dropped abruptly at 55–70 ºC due to glass transition, and then started rising from ~105 ºC owing to the cold crystallization of PLA. Cold crystallization refers to a phenomenon where some amorphous polymers, after heated to temperatures

higher than T_g, are able to crystallize. Below T_g, the E' of PLA/BE blends gradually decreases with increase in BE fractions. When temperature increases, polymer chains start vibrating at around T_g and the chain segmental mobility is stronger at higher temperature. This increased mobility promotes the cold crystallization ability of PLA, which thus increases E'. Very interestingly, cold crystallization moved down to lower temperatures with increase in BE fraction. These results suggested that the incorporation of BE elastomer enhanced the cold-crystallization ability and therefore lowered the cold-crystallization temperature of PLA in the blend. As a result, PLA blends present higher modulus than neat PLA at 95ºC-110 ºC. However, with temperature further increasing, neat PLA crystallizes and therefore demonstrates higher modulus than PLA/BE blends. Finally, E' drops rapidly with temperature over 130 ºC owing to crystal melting.

3.3 Solubility Parameter

Solubility parameter (δ), a measure of the cohesive strength between molecules, is usually used to roughly measure compatibility between polymers [46,47]. δ can be calculated for any molecule from its constituent functional groups:

$$\delta = \left(\frac{E_{coh}}{V}\right)^{1/2} \quad (1)$$

where E_{coh} is the molar attraction constant for a particular functional group with volume V [48]. Solubility parameters of PLA and BE were calculated from Hoftyzer and Van Krevelen's method which is most commonly used for polymers. If the δ difference between the two polymers is less than 0.5, their blends would be miscible. The calculated δ of PLA and BE are 9.64 and 8.94 $(cal/cm^3)^{0.5}$, respectively. the δ difference between PLA and BE is less than 0.5, suggesting that PLA/BE blend is a typical immiscible system; this is in agreement with our previous DMTA analysis.

3.4 Thermal Behavior

Fig. 4 shows the DSC curves of PLA/BE blends, with relevant parameters summarized in Table 1. No crystallization peak was observed from the cooling curves for PLA and its blends. XRD curves (Fig. S2) also illustrated that PLA and its blends were primarily amorphous when cooled from melt at 10 °C/min. These suggest that the PLA/BE blends prepared by melt blending didn't crystallize in time since cooling rate was high (about 30 °C/min, when samples were taken out from hot mold to room temperature for cooling). All the blends show two clear glass transitions, indicating that the two components were phase-separated during cooling. The T_gs of PLA in blends shift to lower temperature with increase in BE fraction, and maximum shift at 22.6 vol% BE display a total 4 °C shift to each other, in line with our afore-mentioned DMTA analysis. Both the heat of cold crystallization (ΔH_{cc}) and the heat of melting (ΔH_m) enhances with increase in BE content, implying that the addition of BE increased the degree of cold crystallization of PLA. The T_g reduction of PLA and the enhanced cold crystallization ability are attributed to the increased segmental mobility of PLA by introducing flexible BE chains.

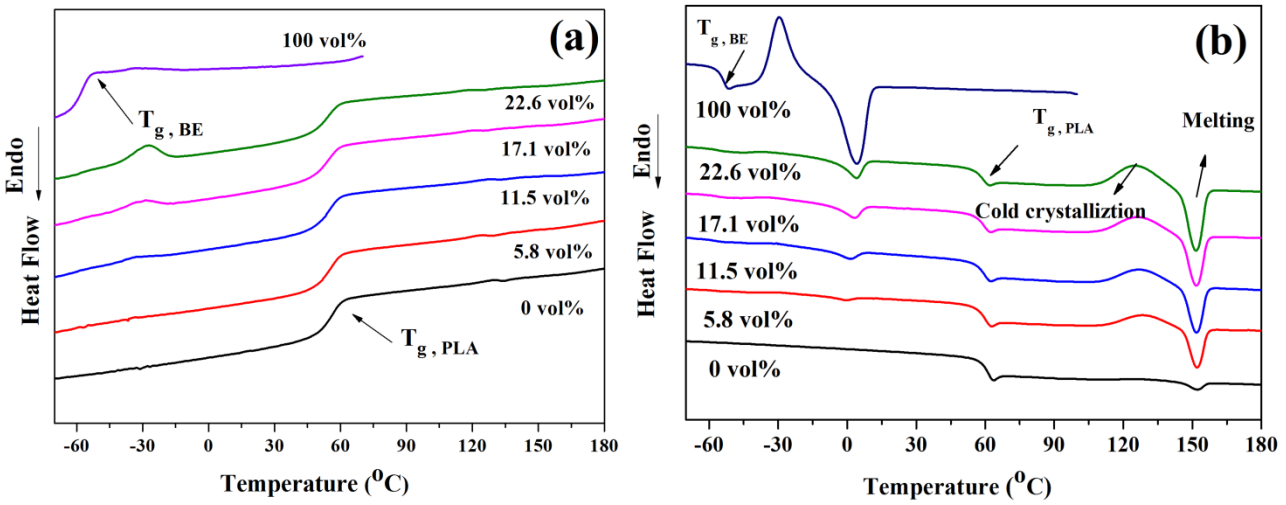

Fig. 4. DSC curves of PLA/BE blends with different amounts of BE:(a) cooling curves; (b) heating curves.

Table 1. Thermal properties of PLA/BE blends with different amounts of BE.

BE (vol%)	BE		PLA						
	$Tg^{a)}$ (°C)	$Tg^{b)}$ (°C)	$T_g^{a)}$ (°C)	$T_g^{b)}$ (°C)	$T_g^{c)}$ (°C)	T_{cc} (°C)	$\triangle H_{cc}$ (J/g)	T_m (°C)	$\triangle H_m$ (J/g)
0	-	-	65.1	59.7	55.3	128.1	0.4	151.9	1.3
5.8	-	-	64.9	58.2	54.7	128.9	6.6	152.0	7.1
11.5	-54.3	-55.8	64.8	57.9	53.6	127.6	8.8	151.5	9.2
17.1	-48.9	-55.4	63.4	57.8	52.9	126.3	10.6	151.5	11.2
22.6	-47.5	-54.5	62.9	57.2	52.2	125.3	14.4	151.4	15.0
100	-	-56.0	-	-	-	-	-	-	-

[a)] Obtained from DMA measurement; [b)] obtained from the heating curves of DSC measurement; [c)] obtained from the cooling curves of DSC measurement; the values of $\triangle H_{cc}$, $\triangle H_m$ were normalized.

Next, the isothermal cold-crystallization behavior of the blends was investigated using isothermal crystallization kinetics. The following Avrami equation was adopted:

$$1 - X_t = \exp(-kt^n) \tag{2}$$

where n is Avrami exponent, and k is the rate constant of crystallization. Both k and n depend on the nucleation and growth mechanisms of spherulites. X_t is the degree of crystallinity at time t. The fraction of X_t is obtained from dividing the area under exothermic peak in DSC isothermal crystallization analysis at a crystallization time t by the total area,

$$X_t = \frac{\int_0^t (dH/dt)dt}{\int_0^\infty (dH/dt)dt} \tag{3}$$

where the numerator is the heat generated at time t and the denominator is the total heat generated up to the complete crystallization.

Equation (4) was obtained by taking the double logarithm of Equation (2):

$$\log[-\ln(1 - X_t)] = \log k + n \log t \tag{4}$$

where log k is the intercept and n is the slope of an Avrami plot. The isothermal crystallization exotherms and the development of crystallinity with time for cold-crystallization of samples were

shown in Fig. S3 and Fig. S4 All isotherms exhibited a sigmoid dependence with time. The plots of log[-ln(1-X_t)] vs log t of PLA with different BE fractions at 125 ºC are plotted in Fig. 5, where each curve exhibits a good linear relationship in agreement with Avrami equation. The n, k, and $t_{1/2}$ values calculated from these lines are summarized in Table S1. The Avrami exponent n varies from 4.5 to 5.0, indicating a three-dimensional crystal growth. The crystallization half-time $t_{1/2}$, the time at which the relative degree of crystallization is 0.5, significantly decreases with addition of BE. These demonstrate that the BE particles increased the crystallization rate of PLA, in agreement with the depressions of T_{cc} and T_g. It is generally accepted that the crystallization kinetics of semicrystalline blends is determined by the chain mobility and intermolecular interactions between two phases [49]. The introducing flexible BE chains increase the PLA chain mobility, and thus enhanced crystallization ability of PLA; but on the other hand the addition of BE enhances molecular interaction between the phases, which restrains PLA crystallization. These two trends are competitive. At 5.8 vol% the chain mobility poses a greater effect on crystallization than the intermolecular interaction between PLA and BE, while at other fractions the improvement of chain mobility might counterbalance the interactions. Thus, the crystallization rate of PLA was little changed with increase in BE fractions.

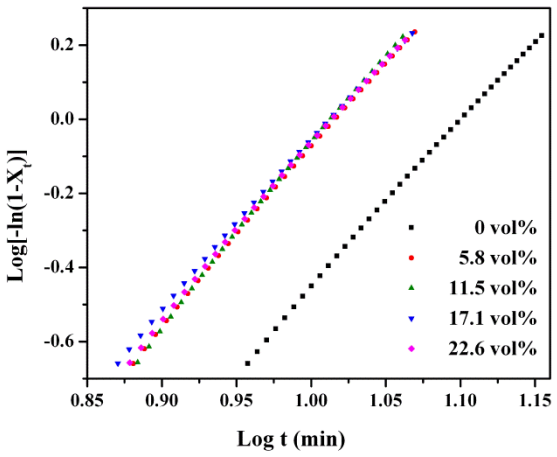

Fig. 5. Effect of different amounts of BE on isothermal crystallization of PLA at 125^{o}C.

3.5 Rheological Properties

To further explore the influence of BE on the melt rheological properties of PLA/BE blends, the oscillatory shear rheological measurements were carried out. The complex viscosity (η^*) of neat PLA and its blends at 170 ºC is shown in Fig. 6a. All materials exhibited a decrease in viscosity with increase in frequency; that is an indication of the shear thinning and also the characteristic of pseudoplastic behavior of polymer blends. It was also observed that BE appeared a higher viscosity and more noticeable shear thinning behavior than PLA. This behavior would be related to relatively high molecular weight and broad molecular weight distribution of BE. As shown in the whole frequency, the viscosities of PLA/BE blends were between the virgin components viscosities, and these values increased as the BE concentration increased. The Newtonian viscosities (η_0) of neat components and blends can be extrapolated by the Carreau model [50] at low frequency. The calculated η_0 from Carreau model of PLA/BE blends were significantly higher than the theoretical ones predicted by the following blend model:

$$\log\ \eta_0 = \phi_1 \log \eta_{01} + \phi_2 \log \eta_{02} \qquad (5)$$

where ϕ is the volume fraction and the subscripts 1 and 2 refer to the two pure components. The η_0 for PLA/BE system (Fig. 6b) showed a positive deviation from the theoretical values, indicating some phase interaction between two components. Such an increase in viscosity for polymer blend was observed for linear low density polyethylene (LLDPE) / cyclo olefin copolymer (COC) blends [51].

Fig. 6c shows the shear storage modulus ($G'(\omega)$) of neat PLA and its blends under oscillatory shear. It can be seen that the $G'(\omega)$ of the PLA/BE blends for every composition are greater than that of pure PLA, and is increasing with the dispersed phase (BE) concentration at a low frequency. The enhancement of blend elasticity over PLA can be attributed to the relaxation of the dispersed phased under slight shear deformation. With increase in BE fraction, it is observed that the diameter of the dispersed phase increase and the relaxation process of the dispersed phase becomes longer, leading to an increase of the storage modulus. $G'(\omega)$ at high frequencies reduced with BE fraction, since highly

deformed BE particles acted as a role of plasticizer. Moreover, the relationship between the storage modulus (G') and the loss modulus (G'') (Han plot) can be used to characterize the miscibility of polymer blends [51,52]. The Han plot of PLA/BE blends is displayed in Fig. 6d. It can be clearly observed that log G'/log G''exhibited linear correlation and close slopes for PLA and 5.8 vol% PLA/BE blend, indicating some compatibility for PLA/BE blend at low concentration of the dispersed phase; other polts showed nonlinear correlation and the shape of them were upturning at low modulus. Nonlinear results indicated that PLA/BE blends are immiscible at high concentration of the dispersed phase.

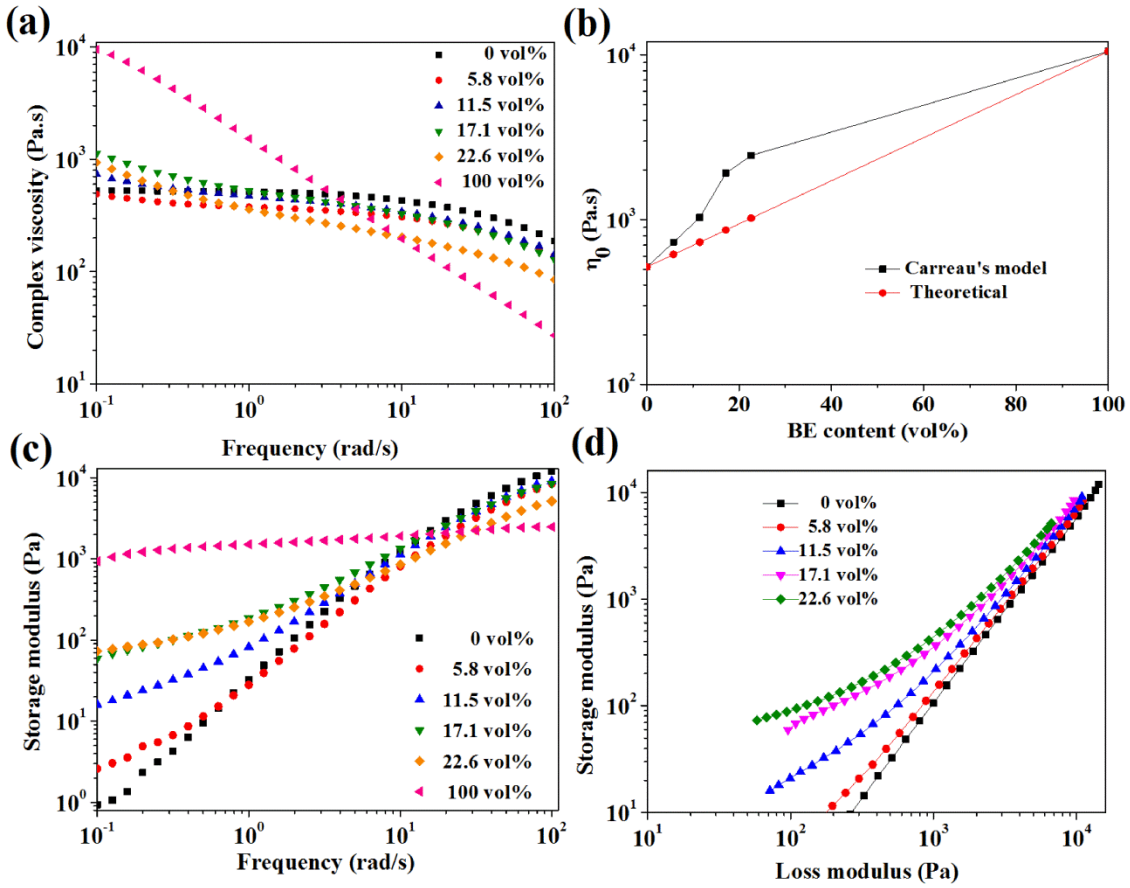

Fig. 6. Rheological properties of PLA/BE blends with different amounts of BE: (a) complex viscosity (η^*); (b) Newtonian viscosities (η_0) vs *compositions*; (c) storage modulus (G'); (d) storage modulus vs loss modulus.

3.6 Toughness and Mechanical Properties

The toughness of a polymer blend/composite can be measure by either tensile testing or impact testing, although the latter is of more popularity. As shown in Fig. 7 the addition of BE changes the tensile behavior of PLA significantly, with details listed in Table S2. Neat PLA fractures at 7 % strain without yielding. By contrast, all blends show distinct yielding which is followed with stable neck growth; these blends are fractured at significantly increased elongation at break in comparison with neat PLA; a brittle-to-ductile transition occurs with increase in BE fractions. The blend containing 11.5 vol% BE shows the highest elongation at break 179 %, nearly 25-fold improvement over neat PLA. Elongation at break enhances with increase in BE fraction until 11.5 vol%, and then decreases obviously. Tensile strength and tensile modulus of blends reduce with BE content, which is reasonable given the low modulus and tensile strength of elastomer.

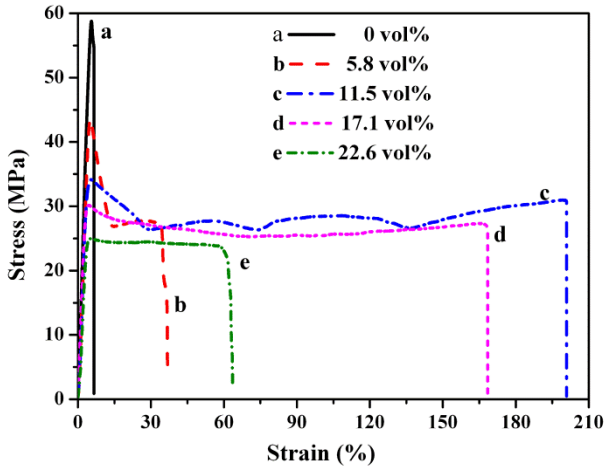

Fig. 7. Typical stress-strain curves of PLA/BE blends with different amounts of BE.

The effect of BE on tensile toughness and notched Izod impact strength is shown in Fig. 8. Tensile toughness—the area under the stress-strain curve of a given material—was a convenient measurement for this material's ductility. It is seen that the tensile toughness of blends increases significantly with BE fractions, and then reduces. The maximum tensile toughness 48.6 MJ/m^3 was reached at 11.5 vol%, 21 fold increase over neat PLA 2.3 MJ/m^3. Notched impact strength represents the ability of a material to absorb fracture energy under a high loading in a notch state; it is a more accurate and more useful

measurement of toughness than the tensile method due to the introduction of a sharp notch. Notched Izod impact strength improves obviously with increase in BE; at 22.6 vol% reached the maximum impact strength 13.4 kJ/m^2, 460% higher than neat PLA (2.4 kJ/m^2). The 11.5 vol% blend seems an optimal composition, inasmuch as a further increase in BE reduces the mechanical properties. Notched Izod impact strength of PLA/BE blend increases to 10.3 kJ/m^2 at 11.5 vol% BE, 330% increment. Compared with petroleum-based toughening, the improvement of impact strength (10.3 kJ/m^2 vs. 2.4 kJ/m^2) may surpass many previous efforts in toughening PLA at similar fractions (Table S3). For instance, Izod impact strength of PLA/poly (butylene adipate-co-terephthalate) (PBAT) blend with 10 wt% PBAT was only 3.0 kJ/m^2 compared with that of 2.6 kJ/m^2 for neat PLA [22]. PLA was blended thermoplastic polyurethane (TPU) elastomer, and the Izod impact strength was improved from 4.0 kJ/m^2 to 5.2 kJ/m^2 at 10wt% TPU [53]. Since a tested value of polymers is known to vary with testing conditions, the comparison herein just provides a rough guide for authors.

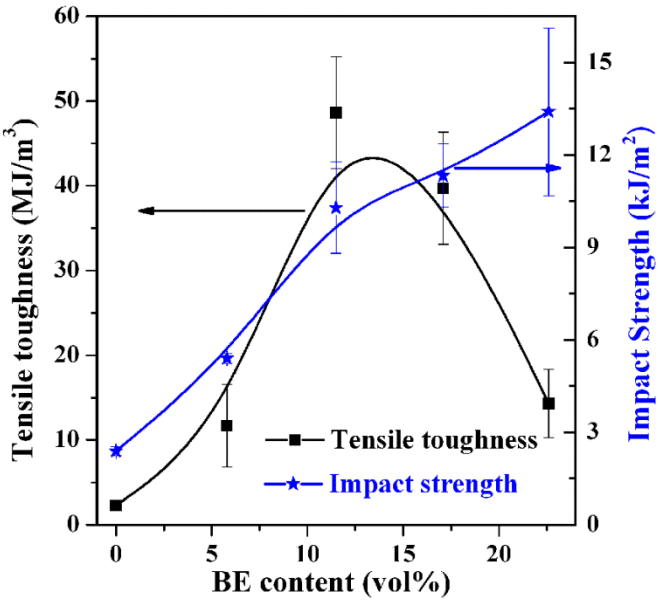

Fig. 8. Effect of BE content in the blends on tensile toughness and impact strength. Bars represent standard deviation of five replicates.

Two reasons for the significantly improved elongation at break and toughness include: (i) uniformly dispersed BE particles in PLA, which upon loading absorbs energy, cavitates and induces matrix shear yielding as to be discussed in 3.7; and (ii) molecular entanglements between PLA and BE chains, which

would be readily generated due to their affinity. The degree of chain entanglement between blend phases is generally determined by their molecular weight and intermolecular interaction such as hydrogen bond; when molecules reach a specific chain length longer than a critical one, these molecules would thus form a coherently entangled physical network [54-55]. Our linear BE polymers of high molecular weight, having a great multitude of bends, twists and kinks, undergo a high level molecular interaction with amorphous PLA macromolecules, which also plays a major role in improving the elongation at break and toughness.

To identify what is caused by the intermolecular interaction between PLA and PE, we designed the following experiment. Both PLA and its 11.5 vol% BE blend were immersed into toluene for 10 min at room temperature. In Fig. 9, holey structure is found for both samples, albeit their structural integrity observed by naked eyes. PLA is amorphous and thus not solvent resistant, so part of PLA would be dissolved by toluene producing holey structure. Upon mixing with BE, no obvious particle is observed in Fig. 2b2, since BE molecules entangled well with PLA; probably part of the entangled PLA/BE macromolecules may anchor either at interface or disperse at sub-micron or even at nanoscale level in matrix. Upon etching, more BE molecules would be dissolved due to their molecular flexibility. Thus more and larger cavities are formed in Fig. 9 than neat PLA and the non-etched blend surface in Fig. 2b2. It is noteworthy that these cavities are interconnected each other, which would be caused by a wide range dispersion of entangled PLA and BE macromolecules. It implies a good level of intermolecular interaction between PLA and BE.

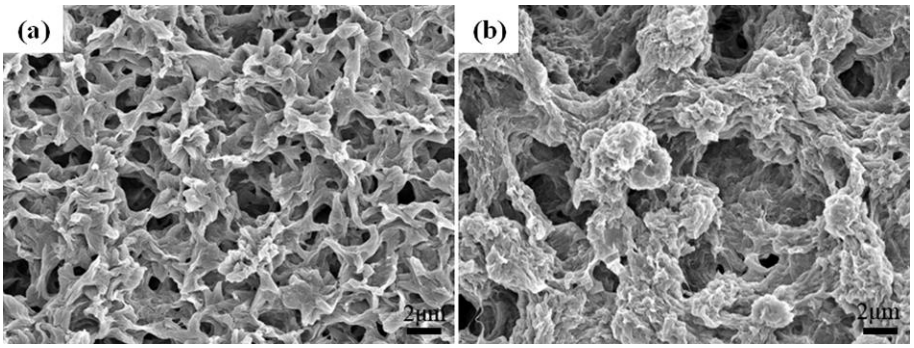

Fig. 9. SEM micrographs of etched samples: (a) PLA; (b) PLA/BE blend (11.5 vol% BE).

3.7 Morphology of Fracture Surface

To further study the toughening effect of PLA/BE blends, the tensile-fractured surfaces were investigated by SEM. In Fig. 10, the surface of neat PLA is flat and mirror-like, indicating a brittle fracture under tensile loading. However, the tensile-fractured surface of the 11.5 vol% blend exhibited fibril-like morphology—evidence of large scale deformation caused matrix shear yielding; these phenomena demonstrate considerable strong interfacial adhesion between PLA and BE phases, leading to a significant improvement of toughness of PLA. Similar behavior was observed before for compatibilized blend [56] and highly toughened epoxy blends [57].

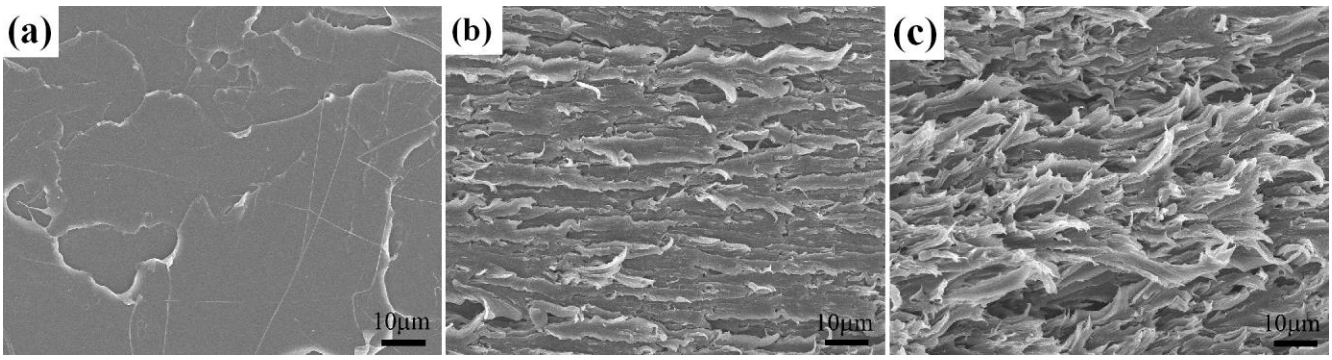

Fig. 10. SEM images of tensile-fractured surface of PLA/BE blends with (a) 0 vol%, (b) 5.8 vol%, (c) 11.5 vol% BE.

Fig. 11 contains SEM micrographs of the impact-fractured surfaces of neat PLA and its 11.5 vol% BE blend. In Fig. 11a, the neat PLA exhibits a smooth surface, indicating brittle failure. The fracture surfaces of the blend exhibited large cavities and a certain degree of matrix deformation, corresponding to ductile fracture. Voids, randomly distributed as dark spots in the micrograph, elongate along the crack propagation. The closer to the fracture surface, the larger size and the more elongated geometry these voids (Fig. 11c, d). Since the BE particles possess far lower strength than PLA matrix, these particles upon loading must cavitate to produce voids; these voids grew along the crack propagation, and by acting as stress concentrators, induced matrix shear yielding which consumed considerable fracture

energy. The size of these cavities is obviously larger than what we measured in morphology investigation by TEM.

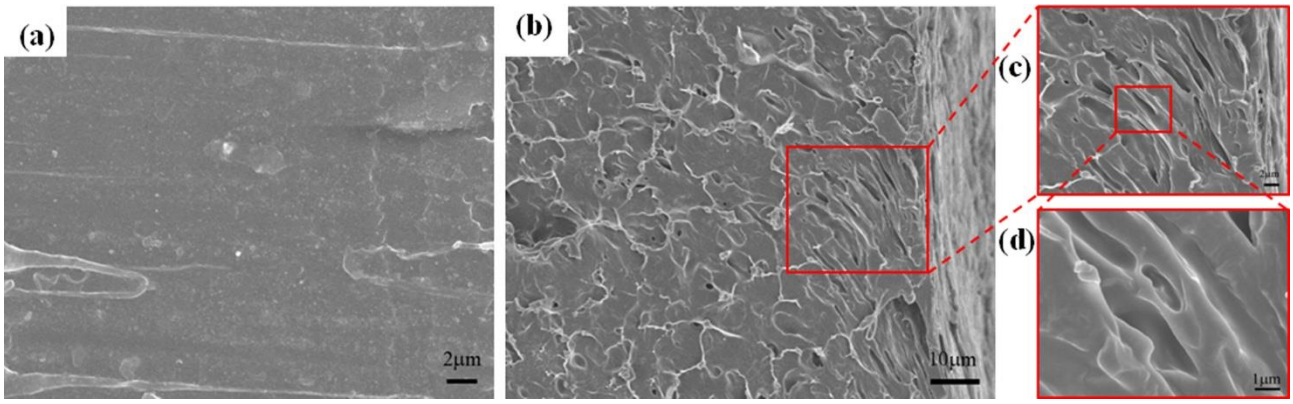

Fig. 11. SEM images of impact-fractured surface of PLA/BE blends with (a) 0 vol%, (b) (c) (d) 11.5 vol% BE.

Conclusions

Polylactide (PLA) was highly toughened by a novel bioelastomer (BE) synthesized from natural renewable resource. Dynamic mechanical thermal analysis (DMTA), differential scanning calorimetry (DSC), transmission electron microscopy (TEM), scanning electron microscopy (SEM) and rheological experiments indicated an improved compatibility for the PLA/BE blends. DSC analyses of the blends revealed that BE dispersion phase enhanced the cold crystallization ability of PLA. Rheological studies revealed that the storage modulus and complex viscosity of the blends were higher than neat PLA at low frequencies. The positive deviation from the theoretical values for η_0 indicated some phase interaction between PLA and BE, which is mainly attributed to molecular similarities since both components are based on ester bond. BE changed the failure behavior of PLA from brittle to ductile according to tensile test and fracture surface micrographs. The optimal BE content for comprehensive properties was found to be 11.5 vol%, at which the blend showed a drastic increase in (i) elongation at break from 7% to 179% and (ii) notched Izod impact strength from 2.4 kJ/m^2 to 10.3 kJ/m^2. SEM micrographs revealed that the toughness improvement is caused by a large-scale matrix deformation which is induced by cavitation of rubber particles. Besides, the *in vitro* cytotoxicity tests showed that these blends are nontoxic towards mouse fibroblasts. Our research indicates that these PLA/BE blends hold great potential for both engineering and biomedical applications.

Acknowledgements

This work was supported by National Natural Science Foundation of China (50933001，51221102), National Outstanding Youth Science Fund (50725310), National Basic Research Program (973 Program) of China (2011 CB606003), and the RCUK China-UK Science Bridges Programme through the Medical Research Council and the Engineering and Physical Sciences Research Council.

Supporting Information Available

The detailed characterizations and discussion about hydrolysis and cytotoxicity test are available in supporting information. Fig. S1, SEM micrographs of (a) PLA/BE blend and (b) PLA/LSR blend; Fig.

S2, XRD patterns of PLA/BE blends with different amounts of BE; Fig. S3, DSC exotherms of isothermal cold-crystallization of PLA/BE blends with different amounts of BE; Fig. S4, Development of crystallinity with time during cold-crystallization; Fig. S5, Mass loss as a function of hydrolysis time at 85^{o}C for PLA, PLA/BE blends; Fig. S6, Viability of L929 mouse fibroblasts as a function of incubation time; Fig. S7, Micrographs comparing morphology of cells after incubation for 3 days conditions: (a) PLA, (b) 11.5 vol% BE, (C) 22.6 vol% BE, (d) BE, (e) Control. Table S1, Isothermal crystallization parameters at 125^{o}C for PLA in the blends; Table S2, Mechanical properties of PLA/BE blends with different amounts of BE; Table S3, Summary of previous effort for toughened PLA using petroleum-based polymers; Table S4, The increase in mass loss of PLA/BE blends with different amounts of BE.

References

[1] Yu L, Deana K, Li L. Prog Polym Sci 2006; 31: 576–602.

[2] Dam JV, Junginger M, Faaij A, Jürgens I, Best G, Fritsche U. Biomass Bioenergy 2008; 32: 749–780.

[3] Chiellini E, Cinelli P, Chiellini F, Iman SH. Macromol Biosci 2004; 4: 218–231.

[4] Williams CK, Hillmyer MA. Polym Rev 2008; 48: 1–10.

[5] Sawyer DJ. Macromol Symp 2003; 201: 271–281.

[6] Drumright RE, Gruber PR, Henton DE. Adv Mater 2000; 12: 1841–1846.

[7] Nijenhuis AJ, Colstee ED, Grijpma W, Pennings AJ. Polymer 1996; 37: 5849–5857.

[8] Martin O, Avérous L.Polymer 2001; 42: 6209–6219.

[9] Kulinski Z, Piorkowska E. Polymer 2005; 46: 10290–10300.

[10] Piorkowska E, Kulinski Z, Galeski A, Masirek R. Polymer 2006; 47: 7178–7188.

[11] Kulinski Z, Piorkowska E, Gadzinowska K, Stasiak M. Biomacromolecules 2006; 7: 2128–2135.

[12] Chen GX, Kim HS, Kim ES, Yoon JS. Polymer 2005; 46: 11829–11836.

[13] Jiang L, Liu B, Zhang J. Ind Eng Chem Res 2009; 48: 7594–7602.

[14] Xu Z, Niu Y, Yang L, Xie W, Li H, Gan Z, Wang Z. Polymer 2010; 51: 730–737.

[15] Hideto T, Yoshito I. J Appl Polym Sci 1996; 60: 2367–2375.

[16] Broz ME, VanderHart DL, Washburn NR. Biomaterials 2003; 24: 4181–90.

[17] HiljanenVainio M, Varpomaa P, Seppälä J, Törmälä P. Macromol Chem Phys 1996; 197: 1503–1523.

[18] Maglio G, Migliozzi A, Palumbo R, Immirzi B, Volpe MG. Macromol Rapid Commun 1999; 20: 236–238.

[19] Wang L, Ma W, Gross RA, McCarthy SP. Polym Degrad Stab 1998; 59: 161–168.

[20] Harada M, Iida K, Okamoto K, Hayashi H, Hirano K. Polym Eng Sci 2008; 48: 1359–1368.

[21] Semba T, Kitagawa K, Ishiaku US, Hamada H. J Appl Polym Sci 2006; 101: 1825–1861.

[22] Jiang L, Wolcott MP, Zhang J. Biomacromolecules 2006; 7: 199–207.

[23] Li Y, Shimizu H. Macromol Biosci 2007; 7: 921–928.

[24] Zhang W, Chen L, Zhang Y. Polymer 2009; 50: 1311–1315.

[25] Ishida S, Nagasaki R, Chino K, Dong T, Inoue Y. J Appl Polym Sci 2009; 113: 558–566.

[26] Huneault MA, Li H. Polymer 2007; 48: 270–280.

[27] Sarazin P, Li G, Orts WJ, Favis BD. Polymer 2008; 49: 599-609.

[28] Liu X, Dever M, Fair N, Benson RS. J Environ Polym Degrad 1997; 5: 225–235.

[29] Shibata M, Inoue Y, Miyoshi M. Polymer 2006; 47: 3557–3564.

[30] Noda I, Satkowski MM, Dowrey AE, Marcott C. Macromol Biosci 2004; 4: 269–275.

[31] Schreck KM, Hillmyer MA. J Biotechnol 2007; 132: 287–295.

[32] Robertson ML, Chang K, Gramlich WM, Hillmyer MA. Macromolecules 2010; 43: 1807–1814.

[33] Stoclet G, Seguela R, Lefebvre JM. Polymer 2011; 52: 1417–1425.

[34] Anderson KS, Schreck KM, Hillmyer MA. Polym Rev 2008; 48: 85–108.

[35] Kinloch AJ, Shaw SJ. Polymer 1983; 24: 1355–1363.

[36] Ratna D. Polymer 2001; 42: 4209–4218.

[37] Jiang W, Tjong SC, Li RKY. Polymer 2000; 41: 3479–3482.

[38] Borggreve RJM, Gaymans RJ, Schuijer J, Ingen Housz JF. Polymer 1987; 28: 1489–1496.

[39] Wei T, Lei L, Kang H, Qiao B, Wang Z, Zhang L, Coates P, Hua K, Kulig J. Adv Eng Mater 2012; 14: 112-118.

[40] Kuan SC.; Dai JB, Du XS, Ma J. Appl Polym Sci 2010; 115: 3265–3267.

[41] Hashima K, Nishitsuji S, Inoue T, Polymer 2010; 51:3934–3939

[42] Ma J, Xu J, Zhu YJ, Zhang LQ. Polymer 2002; 43: 937–945.

[43] Liang JZ, Li RKY. J Appl Polym Sci 2000; 77: 409–417.

[44] Porter RS, Wang LH. Polymer 1992; 33: 2019–2030.

[45] Paul DR, Bucknall CB. Polymer blends, John Wiley & Sons: New York, 2000.

[46] Meaurio E, Zuza E, Sarasua JR. Macromolecules 2005; 38: 1207–1215.

[47] Hansen CM. Prog Org Coat 2004; 51: 77–84.

[48] Van Krevelen DW, te Nijenhuis K. Properties of Polymers, 4nd ed. 2008. pp. 190.

[49] Kuo SW, Chan SC, Chang FC. Macromolecules 2003; 36: 6653–6661.

[50] Carreau PJ, De Kee D, Chhabra R. Munich:Carl Hanser, 1997.

[51] Lamnawar K,Vion-Loisel F, Maazouz A. J. Appl Polym Sci 2010; 116: 2015–2022.

[52] Han CD. J. Appl Polym Sci 1988; 35: 167–213.

[53] Han JJ, Huang HX. J. Appl Polym Sci 2011; 120: 3217–3223.

[54] Follaina N, Jolyb C, Doleb P, Bliarda C. Carbohydr Polym 2005; 60: 185–192.

[55] Carlsson C, Jonsson M. Macromolecules 1996; 29: 7802–7812.

[56] Liang JZ, Li RKY. J Appl Polym Sci 2000; 77: 409–417.

[57] Le QH, Kuan HC, Dai JB, Zaman I, Luong L, Ma J. Polymer 2010; 51: 4867–4879.

Captions of Figures and Tables:

Fig. 1. Chemical structures of (a): Polylactide (PLA) and (b): Bioelastomer (BE).

Fig. 2. Micrographs of PLA/BE blends with (a1, b1) 5.8 vol% BE, (a2, b2) 11.5 vol% BE, (a3, b3) 17.1 vol% BE, and (a4, b4) 22.6 vol% BE. a: TEM micrographs; b: SEM micrographs; D_n: Average particle.

Fig. 3. Dynamic viscoelastic curves of PLA/BE blends with different amounts of BE: (a) tan δ versus temperature; (b) storage modulus versus temperature.

Fig. 4. DSC curves of PLA/BE blends with different amounts of BE: (a) cooling curves; (b) heating curves.

Fig. 5. Effect of different amounts of BE on isothermal crystallization of PLA at 125^{o}C.

Fig. 6. Rheological properties of PLA/BE blends with different amounts of BE: (a) complex viscosity (η^*); (b) Newtonian viscosities (η_0) vs *compositions*; (c) storage modulus (G'); (d) storage modulus vs loss modulus.

Fig. 7. Typical stress-strain curves of PLA/BE blends with different amounts of BE.

Fig. 8. Effect of BE content in the blends on tensile toughness and impact strength. The bar represents standard deviation of five replicates.

Fig. 9. SEM micrographs of etched samples: (a) PLA; (b) PLA/BE blend (11.5 vol% BE).

Fig. 10. SEM images of tensile-fractured surface of PLA/BE blends with (a) 0 vol%, (b) 5.8 vol%, (c) 11.5 vol% BE.

Fig. 11. SEM images of impact-fractured surface of PLA/BE blends with (a) 0 vol%, (b) (c) (d) 11.5 vo% BE.

Table 1. Thermal properties of PLA/BE blends with different amounts of BE.

Supplementary data

Employing a novel bioelastomer to toughen polylactide

Hailan Kang,[†] Bo Qiao,[†] Runguo Wang,[†] Zhao Wang,[†] Liqun Zhang,[,†,‡] Jun Ma,[*,§] Phil Coates[£]*

[†]State Key Laboratory of Organic-Inorganic Composites; [‡]Key Laboratory of Beijing City for Preparation and Processing of Novel Polymer Materials, Beijing University of Chemical Technology, 100029, P. R. China

[§]School of Advanced Manufacturing and Mechanical Engineering, University of South Australia, SA5095, Australia

[£]School of Engineering, Design &Technology, Bradford University, BD7 1DP, UK

CORRESPONDING AUTHOR FOOTNOTE: Correspondences should be addressed to Prof L. Q. Zhang or Dr J. Ma at ZhangLQ@mail.buct.edu.cn or Jun.Ma@unisa.edu.au.

Experimental Section

Hydrolysis test was performed according to ASTM D 3137-81. After treating blends in distilled water at 85 ºC for 5, 10, 15 days in sealed bottles, weight loss was carefully measured. Cell viability was measured using mouse fibroblasts (L-929) by [3-(4, 5-di-methylthiazol-2-yl)-2, 5-diphenyltetrazolium bromide] (MTT) assays. All samples were cut into small slices, sterilized by washing with 75% ethanol, and then rinsed with PBS solution twice. Samples were exposed to Co60 for 15 min and incubated in Dulbecco's modified Eagle's medium (DMEM) at a proportion of 3 cm^2 /ml for 24 h at 37 ºC. The extract solution was then filtered (0.22 μm pore size) to eliminate the possible presence of solid particles of the sample. L929 mouse fibroblasts were grown in DMEM supplemented with 10% fetal bovine serum (FBS) at a density of 5.0×10^4 cells/well and incubated in 5% CO_2 under humidified conditions at 37 ºC. After the incubation, the medium was replaced by the prepared extract dilution which was used as the new culture medium, while the initial medium itself was regarded as a negative control. The cells were allowed to proliferate for 3 days, and the number of viable cells was determined by adding 5 mg/mL MTT in culture medium. After a further incubation of 4 h, the medium was aspirated and the formed blue formazan crystals were dissolved in isopropanol (BDH, Poole, England), and the absorbance at 570 nm was determined. All sample extracts were tested at least three times to obtain consistent results. The relative viability was calculated by,

$$\text{Relative cell viability} = (A_{test} - A_0)/(A_{control} - A_0) \quad (1)$$

$A_{control}$ refers to the absorbance of controlled wells containing cells with DMEM, A_0 refers to the absorbance of the solution containing only DMEM. The morphology incubated 3 days was observed by an inverted phase contrast microscope before the MTT testing.

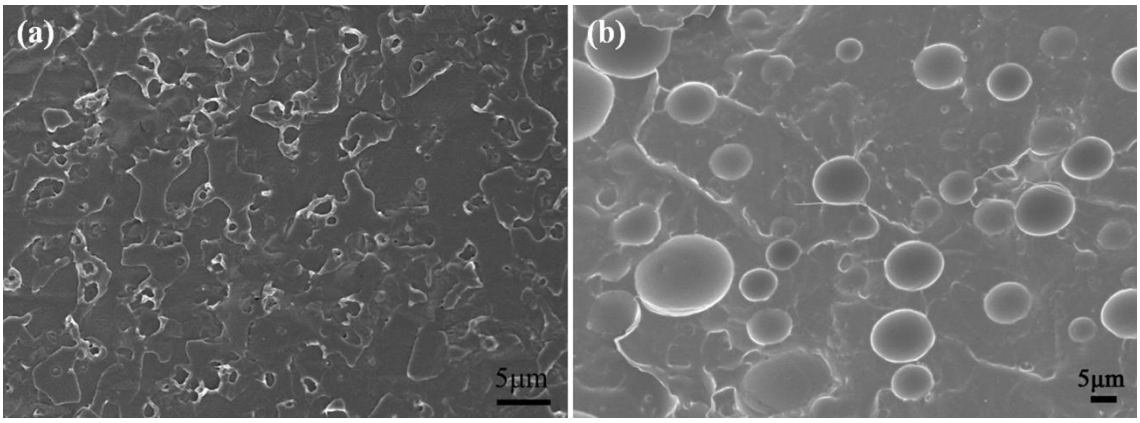

Fig. S1. SEM micrographs of (a) PLA/BE blend (11.5 vol% BE or 10 wt% BE) and (b) PLA/SiR blend (10 wt% SiR).

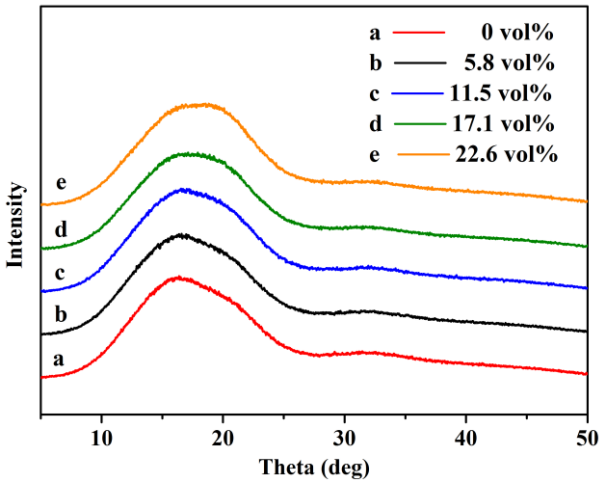

Fig. S2.XRD patterns of PLA/BE blends with different amounts of BE

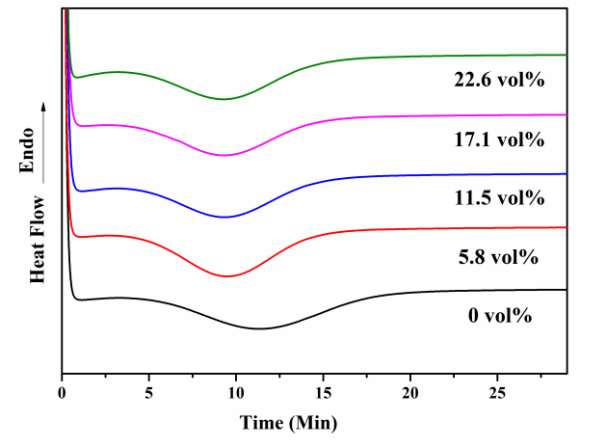

Fig. S3. DSC exotherms of isothermal cold-crystallization of PLA/BE blends with different amounts of BE.

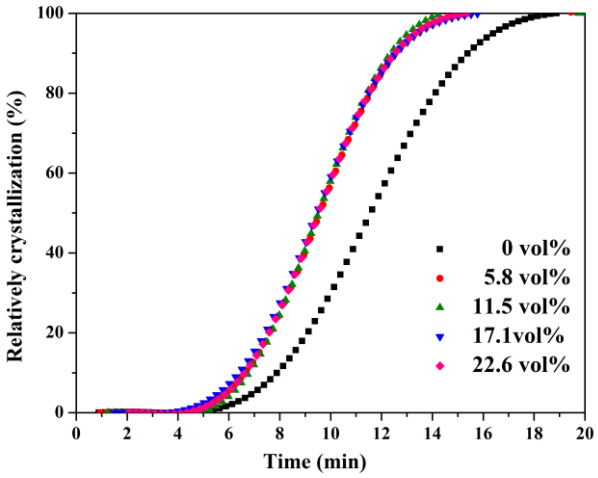

Fig. S4. Development of crystallinity with time during cold-crystallization.

Table S1. Isothermal crystallization parameters at 125^{o}C for PLA in the composites.

BE (vol%)	$t_{1/2}$	k	n
0	11.6	1.23×10^{-5}	4.5
5.8	9.6	1.58×10^{-5}	4.7
11.5	9.5	1.10×10^{-5}	4.9
17.1	9.5	2.75×10^{-5}	4.5
22.6	9.5	1.78×10^{-5}	4.7

Table S2. Mechanical properties of PLA/BE blends with different amounts of BE.

BE (vol%)	Tensile strength (MPa)	Tensile modulus (GPa)	Elongation at break (%)
0	54.0±3.8	1.2±0.09	7±1
5.8	43.5±1.1	1.11±0.07	36±17
11.5	34.3±2.4	1.03±0.05	179±19
17.1	29.4±0.8	0.88±0.09	154±18
22.6	24.3±1.2	0.78±0.08	63±15

Table S3. Summary of previous effort for toughened PLA using petroleum-based polymers.

Name	Content (wt %)	TS (Mpa)	E (Gpa)	ε (%)	IS （kJ/m^2）	Ref
PLA	100	63^{a}	3.4^{a}	3.7^{a}	2.6^{a,c}	1
PBAT	10	55^{a}	2.9^{a}	150^{a}	3.0^{a,c}	1
PLA	100	65	3.5	4	64^{b}	2
PU	10	47	1.8	220	112^{b}	2
PLA	100	59.2^{a}	-	3.7^{a}	-	3
HBP	10	58.5^{a}	-	150^{a}	-	3
PLA	100	46.8	1.8	5.1	-	4
PAE	10	40.9	1.6	194.6	-	4
PLA	100	67.2^{a}	-	13^{a}	4.0^{a,c}	5
TPU	10	53^{a}	-	27^{a}	5.2^{a,c}	5
PLA	100	43^{a}	1.5^{a}	8^{a}	-	6
NBR	10	20^{a}	1.0^{a}	10^{a}	-	6
PLA	100	54.0	1.2	7	2.4^{c}	
BE	10	34.3	1.03	179	10.3^{c}	

PBAT: Poly (butylene adipate-co-terephthalate); PU: Poly (ether) urethane; HBP: Poly (ester amide); PAE: Polyamide elastomer; TPU: thermoplastic polyurethane; TS: Tensile strength; E: Tensile modulus; ε: Tensile elongation at break; IS: Impact strength.

[a] Estimated from graphical data in cited reference, since tabular was not provided.

[b] Impact strength.

[c] Izod impact strength.

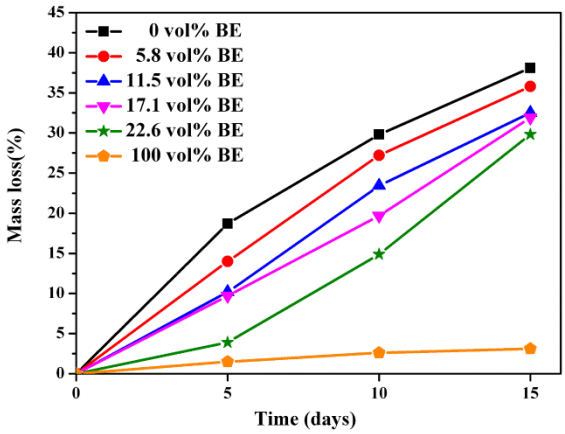

Fig. S5. Mass loss as a function of hydrolysis time at 85°C for PLA, PLA/BE blends.

Upon reaction with water, PLA chains are converted through hydrolysis of ester groups into lactic acid which is biodegradable by microbes, and so it is the density of ester groups that determines the hydrolysis rate. We studied the degradation process by monitoring the mass loss of PLA and its blends after different hydrolysis time. The sample mass loss after different hydrolysis time (m_d) was determined after the samples were dried for 2 days under vacuum at 50 ºC, which was then compared with the initial mass (m_0) according to Equation 2.

$$\Delta m_d\,(\%) = \frac{m_0 - m_d}{m_0} \times 100 \qquad (2)$$

Fig. S5 and Table S4 show the mass loss of the PLA, BE and their blends after different hydrolysis time. The following phenomena are observed: (i) BE exhibits obviously lower mass loss after hydrolysis in comparison with PLA, due to the lower ester bond density of BE macromolecules — our calculation shows 13.89 mmol/g for PLA and 9.88 mmol/g for BE, which obviously relieves the water attack on the ester bonds. (ii) The values of mass loss of all blends generally increase with hydrolysis time as neat

PLA and BE show steady more mass loss with increase in time. (iii) The neat PLA and its blends at 5.8 vol % and 11.5 vol % show lower mass loss rates from 10–15 days than those from 0–5 days, as indicated by the slopes in Fig. S5. By contrast, the blends at higher BE fractions show an opposite trend. This is explained in their molecular structure and blend morphology. Over the first 5 days, the hydrolysis occurs mainly on surface and/or subsurface; since the stiff, homogeneous PLA would not facilitate well the permeation of water molecules into the samples, neat PLA and its low BE content blends show the lower mass loss rate from 10–15 days. Although neat BE shows the lowest mass loss due to its low ester bond density, it actually facilities the permeation of water molecules owing to its ester bonds and elastic nature which means larger free volume than that in a glass state. At 17.1 vol %, the dispersion particles intend to agglomerate to produce a co-continuous phase as shown in Fig. 2b4, forming possible micro-channels for water permeation, and this transfers water molecules into the inner sample producing higher mass loss rate.

Table S4. The increase in mass loss of PLA/BE blends with different amounts of BE.

BE (vol%)	Increase in mass loss (%)		
	0–5 days	5–10 days	10–15 days
0	18.7	11.1	8.3
5.8	14.0	12.9	8.6
11.5	10.2	13.2	9.1
17.1	9.7	10.0	12.2
22.6	3.9	11.0	14.9
100	1.5	1.1	0.5

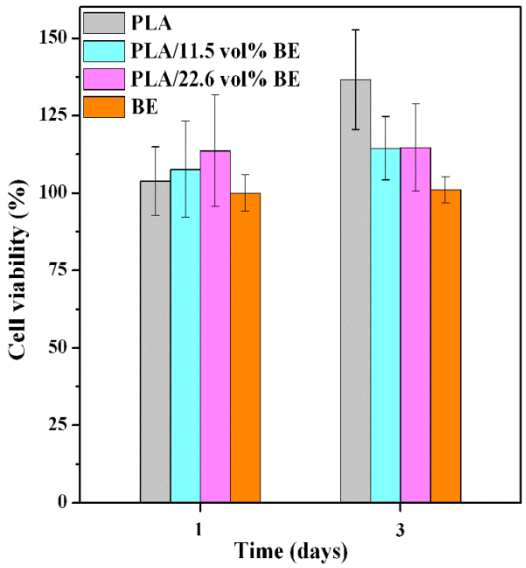

Fig. S6. Viability of L929 mouse fibroblasts as a function of incubation time. The bars represent standard deviation of three replicates

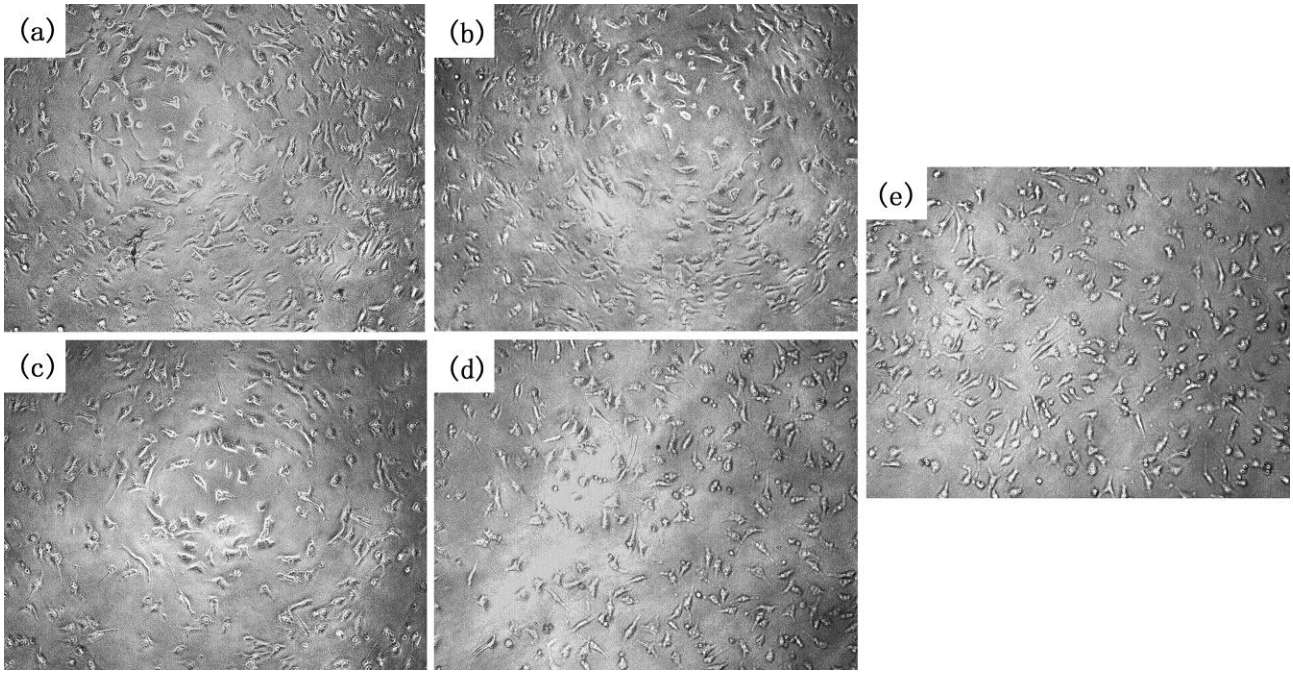

Fig. S7. Micrographs comparing morphology of cells after incubation for 3 days conditions: (a) PLA, (b) 11.5 vol% BE, (C) 22.6 vol% BE, (d) BE, (e) Control.

The cytotoxicity of neat PLA and its blends was evaluated to determine whether they are suitable for biomedical applications. L929 mouse fibroblasts were used in our cytotoxicity assays owing to their popularity and three days was chosen as the incubation period to allow for the completion of at least one cell cycle. A material would be considered as nontoxic when its cell viability is at least 75 % higher than

the control. In Fig. S6, the cell proliferation values for neat PLA and BE were approximately 137% and 101% over the control sample, respectively, showing that both polymers have acceptable biocompatibility. The cell viabilities of all blends are higher than 100 %. As seen in Fig. S7, L929 cells show a normal stellate morphology and exhibit no negative response to any samples after the incubation 3 days, implying the nontoxicity of all samples tested.

References

[1] Jiang L, Wolcott MP, Zhang J. Biomacromolecules 2006; 7: 199–207.

[2] Li Y, Shimizu H. Macromol Biosci 2007; 7: 921–928.

[3] Lin Y, Zhang KY, Dong ZM, Dong LS, Li YS. Macromolecules 2007, 40: 6257–6267.

[4] Zhang W, Chen L, Zhang Y. Polymer 2009; 50: 1311–1315.

[5] Han JJ, Huang HX. J. Appl Polym Sci 2011; 120: 3217–3223.

[6] Ishida S, Nagasaki R, Chino K, Dong T, Inoue Y. J Appl Polym Sci 2009; 113: 558–566.